## A NUMERICAL SCHEME FOR WAVE TURBULENCE: 3-WAVE KINETIC EQUATIONS $^*$

STEVEN WALTON† AND MINH-BINH TRAN‡

Dedicated to the 70th Birthday of Professor Duong Minh Duc

**Abstract.** We introduce a finite volume scheme to solve a special case of isotropic 3-wave kinetic equations. We test our numerical solution against theoretical results concerning the long time behavior of the energy and observe that our solutions verify the energy cascade phenomenon. To our knowledge, this is the first numerical scheme that can capture the long time asymptotic behavior of solutions to those isotropic 3-wave kinetic equations, where the energy cascade can be observed. Our numerical energy cascade rates are in good agreement with previously obtained theoretical results. The finite volume scheme given here relies on a new identity, allowing one to reduce the number of terms needed in the collision operators.

 $\mathbf{Key}$  words. wave turbulence, 3-wave equation, partial differential equations, finite volume method

MSC codes. 65M08, 45K05, 76F55

**DOI.** 10.1137/22M1492210

1. Introduction. For more than 60 years, the theory of weak wave turbulence has been intensively developed. Having origins in the works of Peierls [32, 33], with modern developments originating in the works of Hasselman [17, 18], Benney and Saffmann [4], Kadomtsev [22], Zakharov, L'vov, and Falkovich [45], and Benney and Newell [3], wave turbulence kinetic equations have been shown to play an important role in a vast range of physical applications. Well-known examples are water surface gravity and capillary waves, internal waves on density stratification, inertial waves due to rotation in planetary atmospheres and oceans, waves on quantized vortex lines in superfluid helium, and planetary Rossby waves in weather and climate evolution.

In rigorously deriving wave turbulence kinetic equations, Lukkarinen and Spohn are pioneers with the work [27]. In the last few years, the rigorous justification of wave turbulence theory has been revisited in [5, 6, 11, 12, 40] in an effort to tackle the longstanding open conjecture on the long time behavior of higher order Sobolev norms,  $H^s$  (s > 1), of solutions to dispersive equations on the torus.

The 3-wave kinetic equation, one of the most important classes of wave kinetic equations, reads (see [35, 36, 43, 44, 46])

(1.1) 
$$\partial_t f(t, p) = \mathcal{Q}[f](t, p), f(0, p) = f_0(p),$$

 $\rm https://doi.org/10.1137/22M1492210$ 

**Funding:** The authors are funded in part by NSF RTG grant DMS-1840260, NSF grants DMS-1854453, DMS-2204795, and DMS-2305523, by a Humboldt Fellowship, and by NSF CAREER grants DMS-2044626 and DMS-2303146.

B467

<sup>\*</sup>Submitted to the journal's Computational Methods in Science and Engineering section April 25, 2022; accepted for publication (in revised form) February 24, 2023; published electronically July 7, 2023.

<sup>&</sup>lt;sup>†</sup>Department of Mathematics, Southern Methodist University, Dallas, TX 75275 USA. Current address: XCP-4, Los Alamos National Laboratory, Los Alamos, NM 87544 USA (stevenw@smu.edu).

<sup>&</sup>lt;sup>†</sup>Department of Mathematics, Texas A&M University, College Station, TX 77843 USA (minhbinh@tamu.edu).

in which f(t,p) is the nonnegative wave density at wavenumber  $p \in \mathbb{R}^N$ ,  $N \geq 2$ ;  $f_0(p)$  is the initial condition. The quantity  $\mathcal{Q}[f]$  describes pure resonance and is of the form

$$(1.2) \mathcal{Q}[f](p) = \iint_{\mathbb{R}^{2N}} \left[ \mathcal{R}_{p,p_1,p_2}[f] - \mathcal{R}_{p_1,p,p_2}[f] - \mathcal{R}_{p_2,p,p_1}[f] \right] d^N p_1 d^N p_2,$$

with

$$\mathcal{R}_{p,p_1,p_2}[f] := |V_{p,p_1,p_2}|^2 \delta(p - p_1 - p_2) \delta(\omega - \omega_1 - \omega_2) (f_1 f_2 - f f_1 - f f_2),$$

with the shorthand notation f = f(t,p),  $\omega = \omega(p)$  and  $f_j = f(t,p_j)$ ,  $\omega_j = \omega(p_j)$  for wavenumbers  $p, p_j, j \in \{1,2\}$ . The function  $\omega(p)$  is the dispersion relation of the wave system. The 3-wave kinetic equation has a variety of application areas, including ocean waves, acoustic waves, gravity capillary waves, Bose–Einstein condensates, and many others (see [17, 18, 34, 42, 43, 44] and references therein).

In the isotropic case, we identify f(t,p) with  $f(t,\omega)$ ; the isotropic 3-wave kinetic equation, in which only the forward transferring part of the collision operator is considered, takes the form

$$(1.3) \\ \partial_t f(t,\omega) = Q[f](t,\omega), \quad \omega \in \mathbb{R}_+, f(0,p) = f_0(p), \\ Q[f](t,\omega) = \int_0^\infty \int_0^\infty \left[ R(\omega,\omega_1,\omega_2) - R(\omega_1,\omega,\omega_2) - R(\omega_2,\omega_1,\omega) \right] d\omega_1 d\omega_2, \\ R(\omega,\omega_1,\omega_2) := \delta(\omega - \omega_1 - \omega_2) \left[ U(\omega_1,\omega_2) f_1 f_2 - U(\omega,\omega_1) f f_1 - U(\omega,\omega_2) f f_2 \right],$$

where U satisfies  $|U(\omega_1, \omega_2)| = (\omega_1 \omega_2)^{\gamma/2}$ , in which  $\gamma$  is a nonnegative constant, which plays an important role in what follows. Note that the operator Q[f] can be considered as a coagulation kinetic type operator for wave interactions.

One of the breakthrough results in weak turbulence theory (see [24, 44, 45]) concerns the existence of the so-called Kolmogorov–Zakharov (KZ) spectra, which is a class of *time-independent solutions*  $f_{\infty}$  of equation (1.1):

$$f_{\infty}(p) \approx C|p|^{-\kappa}, \quad \kappa > 0.$$

The KZ solutions are analogous to the Kolmogorov energy spectrum of hydrodynamic turbulence, though the value of  $\kappa$  in weak turbulence theory is dependent upon the wave system under consideration. Research in line with this topic has actively continued to the present (see, for instance, [15, 28, 29], to name only a few). However, in the absence of forcing and dissipation, the KZ solution scaling is only expected for infinite capacity systems, e.g., for a forward cascade process whose energy integral diverges at infinite p. In the opposite case of finite capacity systems, the spectrum blows up in finite time. The systems we consider in the present article are of the latter class.

To our knowledge, relatively little has been done on the time-dependent solutions of (1.1). In the important works [7, 8, 9], several numerical experiments were designed for investigating the isotropic 3-wave equation. In [7], it was pointed out that isotropic 3-wave kinetic equations are equivalent to mean field rate equations for an aggregation-fragmentation problem which possesses an unusual fragmentation mechanism. A numerical method for solving isotropic 3-wave kinetic equations, with forcing and dissipation present, was also introduced in the same work.

In [39], Soffer and Tran show that the energy conserved isotropic solutions of (1.1) in the finite capacity case (with  $\gamma > 1$ ) exhibit the property in which energy is cascaded from small wavenumbers to large wavenumbers. They show that for a

regular initial condition whose energy at infinity,  $\omega = \infty$ , is initially 0, as time evolves the energy is gradually accumulated at  $\{\omega = \infty\}$ . In the long time limit, all the energy of the system is concentrated at  $\{\omega = \infty\}$ , and the energy function becomes a Dirac function at infinity  $\mathcal{E}\delta_{\{\omega=\infty\}}$ , where  $\mathcal{E}$  is the total energy. To be more precise, let us define the energy of the solution (1.1) as  $g(t,\omega) = \omega f(t,\omega)$ . It has been proved in [39] that g can be decomposed into two parts,

(1.4) 
$$g(t,\omega) = \bar{g}(t,\omega) + \tilde{g}(t)\delta_{\{\omega=\infty\}},$$

where  $\bar{g}(t,\omega) \geq 0$  is the regular part, which is a function, and  $\tilde{g}(t)\delta_{\{\omega=\infty\}}$  is the singular part, which is a measure. The function  $\tilde{g}(t)$  is nonnegative. Initially,  $\bar{g}(0,\omega) = g(0,\omega)$  and  $\tilde{g}(0) = 0$ . But there exists a blow-up time  $t_1^*$  such that for all time  $t > t_1^*$ , the function  $\tilde{g}(t)$  is strictly positive. Moreover, starting from time  $t_1^*$ , there exists infinitely many blow-up times,

$$(1.5) 0 < t_1^* < t_2^* < \dots < t_n^* < \dots,$$

such that

$$(1.6) \bar{g}(t_1^*, \omega) > \bar{g}(t_2^*, \omega) > \dots > \bar{g}(t_n^*, \omega) > \dots \to 0$$

and

$$(1.7) 0 < \tilde{g}(t_1^*) < \tilde{g}(t_2^*) < \dots < \tilde{g}(t_n^*) < \dots$$

This phenomenon has been explained in [39]: after the first blow-up time,  $t_1^*$ , the energy starts to transfer from the regular part  $\bar{g}(t,\omega)$  to the singular part  $\tilde{g}(t)\delta_{\omega=\infty}$  at a rate of at least  $\mathcal{O}(\frac{1}{\sqrt{t}})$ , while the total energy of the two regular and singular parts is still conserved. This decay rate has been obtained in item (iii) of the main theorem of [39] (Theorem 10, pp. 22–45), which is stated as follows. The energy cascade has an explicit rate  $\int_{\{|p|=\infty\}} f(t,|p|)\omega_{|p|}|p|^2d\mu(|p|) \geq \mathfrak{C}_1 - \frac{\mathfrak{C}_2}{\sqrt{t}}$ , where  $\mathfrak{C}_1$  and  $\mathfrak{C}_2$  are explicit constants. Item (iii) of the main theorem states that the total energy is accumulated at the point  $\{\infty\}$  with the rate  $\mathcal{O}(\frac{1}{\sqrt{t}})$ . The above inequality yields with  $\omega=|p|$  the equivalent rate

$$\int_0^R g(t,\omega)d\omega \le \mathcal{O}\left(\frac{1}{\sqrt{t}}\right) \text{ for any } R > 0.$$

In the limit  $t \to \infty$ , all of the energy will be accumulated in the singular part  $\tilde{g}(t)\delta_{\omega=\infty}$ , while the regular part  $\bar{g}(t,\omega) \to 0$  will vanish. This means that if we look for a strong (nonmeasured) solution whose energy is conserved, then it can only exist up to a very short time  $t=t_1^*$ , at which point it exhibits singular behavior. As a result, we refer to time  $t_1^*$  as the first blow-up time. Let  $\chi_{[0,R]}(\omega)$  be a cut-off function of  $\omega$  on the finite domain [0,R]; the multiple blow-up time phenomenon (1.4)–(1.5)–(1.6)–(1.7), with the decay rate  $\mathcal{O}(\frac{1}{\sqrt{t}})$ , can be observed equivalently as the decay of the total energy on any finite interval [0,R],

$$\int_0^R \!\!\! g(t,\omega) d\omega = \!\! \int_{\mathbb{R}_+} \!\! \chi_{[0,R]}(\omega) g(t,\omega) d\omega \leq \mathcal{O}\Big(\frac{1}{\sqrt{t}}\Big) \text{ as } t \to \infty \text{for all truncated parameter} R.$$

Inequality (1.8) simply means that the energy of the solution will move away from any truncated finite interval [0, R] as  $t \to \infty$  with the rate  $\mathcal{O}\left(\frac{1}{\sqrt{t}}\right)$ .

We refer the reader to [39] for a detailed comparison of the different results of [7, 8, 9, 39]. Below, a brief comparison will be given. In [7, 8, 9], both the infinite capacity  $(0 \le \gamma \le 1)$  and finite capacity  $(\gamma > 1)$  cases have been considered. The solutions of [8, 9] are assumed to follow a self-similar hypothesis, called dynamic scaling,

(1.9) 
$$f(t,\omega) \approx s(t)^a F\left(\frac{\omega}{s(t)}\right),$$

where  $\approx$  denotes the scaling limits  $s(t) \to \infty$  and  $\omega \to \infty$  with  $x = \omega/s(t)$  fixed. The energy of this function can be computed as

$$\int_{0}^{\infty} \omega f(t,\omega) d\omega = \int_{0}^{\infty} s(t)^{a} F\left(\frac{\omega}{s(t)}\right) \omega d\omega = \int_{0}^{\infty} s(t)^{a+2} F\left(\frac{\omega}{s(t)}\right) \left(\frac{\omega}{s(t)}\right) d\left(\frac{\omega}{s(t)}\right) d\left(\frac{\omega}{s(t)}\right) ds = s(t)^{a+2} \int_{0}^{\infty} x F(x) dx \sim \mathcal{O}\left(s(t)^{a+2}\right),$$

which grows with the rate  $s(t)^{a+2}$ . Substituting this ansatz into (1.3), we obtain the system

(1.11) 
$$\dot{s}(t) = s^{\zeta} \text{ with } \zeta = \gamma + a + 2 \text{ and } aF(x) + x\dot{F}(x) = Q[F](x).$$

From (1.10), it can be observed that the only value of a that gives the conservation of energy is a=-2. Making the assumption that  $F(x) \backsim x^{-n}$ , when  $x\backsim 0$ , this work shows that the power can be determined to be  $n=\gamma+1$ . Since [8] focuses on the infinite capacity case, the degree of homogeneity  $\gamma$  is considered in the interval [0,1); thus the integral

is well-defined. However, there is a problem in the finite capacity case: when  $\gamma > 1$ , this integral becomes singular.

The work [9] considers both infinite capacity  $(0 \le \gamma \le 1)$  and finite capacity  $(\gamma > 1)$  cases. In the finite capacity case, the solution is considered before the first blow-up time  $t < t_1^*$ , theoretically proved in [39]. However, solving (1.11) is a very difficult task. In [9], the following hypothesis is then needed: the total energy of the solution of (1.3) is assumed to grow linearly in time rather than being conserved, so that

(1.13) 
$$\int_{0}^{\infty} \omega f(t,\omega) d\omega = Jt.$$

Another challenging technical issue is that the integration (1.12) with  $F(x) \sim x^{-\frac{\gamma+3}{2}}$  for small x diverges in the finite capacity case  $(\gamma > 1)$  and converges only in the infinite capacity case  $(0 \le \gamma \le 1)$ . Thus, other assumptions need to be imposed on the solution f itself.

From the above discussions, the key differences between [7, 8, 9] and [39] are summarized as follows. The works complement one another, as they consider very different scenarios of the solutions of (1.1). The work [39] focuses on the finite capacity case ( $\gamma > 1$ ), under no additional assumption on the solution f of (1.3), and shows that the solution, whose energy is conserved rather than linearly growing in time

as assumed in (1.13), exhibits an energy cascade phenomenon, where there exist an infinite series of blow up times (1.4)-(1.5)-(1.6)-(1.7) (or, equivalently, inequality (1.8)). The result of [39] is in good agreement with the discussion of [30], saying that in the absence of external forcing and dissipation, the KZ spectrum is not expected in the finite capacity  $(\gamma > 1)$  case. The works [7, 8, 9] focus on both finite capacity  $(\gamma > 1)$  and infinite capacity  $(0 \le \gamma \le 1)$  cases. In the finite capacity case  $(\gamma > 1)$ , the solution is studied before the first blow-up time  $t < t_1^*$ , rigorously proved later in [39]. Studying the solution before the first blow-up time via the self-similar hypothesis (1.9) is indeed a highly challenging problem, and thus in [9] the following assumption needs to be imposed on the energy of the solution: it is assumed to grow linearly in time (see (1.13)) rather than being conserved, so that

(1.14) 
$$\int_0^\infty \omega f(t,\omega) d\omega = \text{ constant.}$$

Moreover, additional hypotheses are also imposed to treat the singularities of the integral (1.12).

We would like to highlight the work [2], where a self-similar profile of the solution for a different finite capacity system—the Alfven wave turbulence kinetic equation—is computed before the first blow-up time  $t_1^*$ . Also, the recently published paper [38] presents a numerical method for solving the self-similar profile before the first blow-up time  $t_1^*$  for a collision integral 4-wave kinetic equation based on Chebyshev approximations. While finding self-similar profiles of the solution f of (1.1) not only before the first blow-up time  $t_1^*$  but also before the nth blow-up time  $t_n^*$  is a topic of our future work, our current paper only focuses on numerically verifying the existence of the multiple blow-up time  $t_1^* < t_2^* < \cdots < t_n^* < \cdots$  phenomenon as well as the bound (1.8), rigorously proved in [39].

Let us also mention the work [37], where a 3-wave kinetic equation, derived from the elastic beam wave equation on the lattice, has been analyzed. It has been shown that the domain of integration of the 3-wave collision operator is broken into disconnected domains, where each has its own local equilibrium. If one starts with any initial condition, whose energy is finite on one subdomain, the solutions will relax to the local equilibrium of this subregion as time evolves. This is the so-called nonergodicity phenomenon, which is different from the energy cascade phenomenon observed in our current work. The global existence of 3-wave kinetic equations in the presence of forcing has been shown in [16, 31], and a connection to chemical reaction networks has also been pointed out in [41].

Starting from (1.3), we could rewrite the 3-wave kinetic equation under the equivalent form

(1.15) 
$$\partial_t f(t,k) = \mathbb{Q}[f](t,k), \quad k \in \mathbb{R}_+, \ f(0,k) = f_0(k),$$

in which  $\mathbb{Q}$  is the collision operator defined by

$$(1.16) \qquad \mathbb{Q}[f](t,k) = \int_0^k [a(k_1, k - k_1)f(k_1)f(k - k_1) - a(k, k_1)f(k)f(k_1) - a(k, k - k_1)f(k)f(k - k_1)] dk_1 - 2 \int_0^\infty [a(k, k_1)f(k)f(k_1) - a(k + k_1, k_1)f(k + k_1)f(k_1) - a(k, k_1 + k)f(k)f(k_1 + k)] dk_1,$$

where the collision kernel satisfies  $a(k_1, k_2) = (k_1 k_2)^{\gamma/2}$ . In the rest of our paper, we identify the variable k with the variable  $\omega$  as k is simply  $\omega$  multiplied by a fixed constant.

Even though the theoretical result of [39] holds for the more general equation (1.1) in the isotropic case, it is expected that the result also hold for equation (1.3), in which only the part that drives the forward cascade is kept. Therefore, the goal of our paper is then to derive a finite volume scheme (FVS) that allows us to observe the time evolution of the solutions of (1.15) and to verify the theoretical results of [39] for various values of  $\gamma > 1$ . In other words, we aim to observe the transferring of energy from the regular to the singular part in (1.4) and to measure precisely the rate of this energy transfer process via the inequality (1.8), which we call the energy cascade rate. In the absence of forcing and dissipation, the KZ spectrum is not expected in the finite capacity ( $\gamma > 1$ ) case considered in our current work [30].

Our FVS relies on the combination of a new energy identity represented in Lemma 2.1 and an adaptation of Filbet and Laurençot's scheme [13] for the Smoluchowski coagulation equation (SCE) to the 3-wave kinetic equation. Most numerical schemes that approximate integrals on an unbounded domain require the truncation of the unbounded domain to a finite domain. Thanks to the new identity, the number of terms in the collision operators is reduced, which reduces the number of truncations needed in the approximation, making the scheme more accurate and reliable. Indeed, we only need to truncate one term in our numerical scheme. Let us comment that the CFL condition is restrictive in certain cases. For other types of equations, the issue of positivity and accurate long time behavior could be resolved by using the implicit in time discretizations. For instance, a structure preserving scheme has been designed for the Kolmogorov-Fokker-Planck equation, which is an equation of degenerate parabolic type in the work [14].

The advantage of degenerate parabolic type equations is that those equations are normally local, while the 3-wave kinetic equation considered in the current paper is highly nonlocal. Thus, the previous strategies for parabolic equations, such as the one used for the above Kolmogorov–Fokker–Planck equation, do not immediately carry over to the current 3-wave kinetic equation. We therefore defer this question to a future paper.

2. Comparison with Smoluchowski Coagulation Equation and a New Energy Identity. In [13], Filbet and Laurençot derive an FVS for the SCE

(2.1) 
$$\partial_t f(t,k) = \mathbb{Q}_{Smo}[f](t,k), \ f(0,k) = f_0(k),$$

(2.2)

$$\mathbb{Q}_{Smo}[f](t,k) = \int_0^k a(k_1,k-k_1)f(k_1)f(k-k_1)dk_1 - 2\int_0^\infty a(k,k_1)f(k)f(k_1)dk_1,$$

where  $a(\cdot, \cdot)$  is the collision kernel for the 3-wave collision operator (1.16). Let us give a short derivation of the nonconservative form of the SCE (see [1, 10, 13] and the references therein).

Take a test function  $\phi(k) = k\chi_{[0,c]}(k)$  and apply it to the SCE

$$\int_{0}^{c} \partial_{t} f(t,k) k dk = \int_{0}^{c} \int_{0}^{k} a(k,k-k_{1}) f(k_{1}) f(k-k_{1}) k dk_{1} dk$$
$$-2 \int_{0}^{c} \int_{0}^{\infty} a(k,k_{1}) f(k) f(k_{1}) k dk_{1} dk$$

$$=2\int_{0}^{c}\int_{0}^{c-k}a(k,k_{1})f(k)f(k_{1})k\mathrm{d}k_{1}\mathrm{d}k-2\int_{0}^{c}\int_{0}^{\infty}a(k,k_{1})f(k)f(k_{1})k\mathrm{d}k_{1}\mathrm{d}k.$$

Rearranging the right-hand side, we find

$$\int_0^c \partial_t f(t,k) k \mathrm{d}k = -2 \int_0^c \int_{c-k}^\infty a(k,k_1) f(k_1) f(k) k \mathrm{d}k_1 \mathrm{d}k;$$

upon taking the derivative with respect to c,

$$\partial_t f(t,c)c = -2\partial_c \int_0^c \int_{c-k}^{\infty} a(k,k_1)f(k_1)f(k)k dk_1 dk;$$

and, after truncating the inner integral, we arrive at

(2.3) 
$$\partial_t f(t,c)c = -2\partial_c \int_0^c \int_{c-k}^R a(k,k_1)f(k_1)f(k)k dk_1 dk,$$

where R is a suitable truncation of the volume domain. Then, one can apply any FVS scheme to solve the truncated problem. We note briefly that the choice of R can affect the accuracy and efficiency of the scheme for the SCE. For example, when considering the case of gelation, R must be quite large in order to avoid a loss of mass before the gelation time. Also, in [23] the authors compare the FVS above with a finite element approximation and find that for smaller truncation values, the finite element scheme is a better choice, while for larger truncation values the FVS should be used.

If we compare (1.16) with (2.2), we see that the SCE is a special case of the 3-wave equation. Thus, we would like to adapt the FVS of Filbet and Laurençot to derive a numerical scheme for the 3-wave equation. To do this we derive an identity similar to (2.3) for the wave kinetic equation. The role of this identity is to reduce the number of terms in the collision operator. As discussed previously, the truncation of the terms in the collision operator can affect the accuracy of the numerical scheme; thus reducing the number of truncated terms is crucial in the numerical computations of the solutions, as it allows the scheme to be more accurate and reliable.

However, for the 3-wave equation the wave density, f(t,k), is not conserved, but the energy, g(t,k) = kf(t,k), is conserved, and so we solve for the energy. What's more, since we do not have an analytic solution to test against, we validate our scheme by verifying the energy cascade rate for the 3-wave equation found in Soffer and Tran [39] and discussed above.

LEMMA 2.1. The following identity holds true for the energy function q(t,k):

(2.4) 
$$\partial_{t} \frac{g(t,c)}{c} = -2\partial_{c} \int_{0}^{c} \int_{0}^{c} a(k,k_{1}) \frac{g(k)}{k} \frac{g(k_{1})}{k_{1}} \chi\{c < k + k_{1}\} dk_{1} dk + \partial_{c} \int_{0}^{\infty} \int_{0}^{\infty} a(k,k_{1}) \frac{g(k)}{k} \frac{g(k_{1})}{k_{1}} \chi\{c < k + k_{1}\} dk dk_{1},$$

with  $\chi\{\cdot\}$  the characteristic function and initial condition  $g(0,k) = g_0(k) = kf(0,k)$ .

*Proof.* Let  $\phi(k)$  be a test function. From [39], we have the following identity for the 3-wave equation:

$$\int_{0}^{\infty} \partial_{t} f(t,k) \phi(k) dk = \int_{0}^{\infty} \int_{0}^{\infty} a(k,k_{1}) f(k) f(k_{1}) [\phi(k+k_{1}) + \phi(|k-k_{1}|) - 2\phi(\max\{k,k_{1}\})] dk dk_{1}.$$
(2.5)

If we choose  $\phi(k) = \chi_{[0,c]}(k)$  (compare this with  $\phi(k) = k\chi_{[0,c]}(k)$  in [13]), we have

$$\int_{0}^{\infty} \partial_{t} f(t,k) \chi_{[0,c]}(k) dk = \int_{0}^{\infty} \int_{0}^{\infty} a(k,k_{1}) f(k) f(k_{1}) [\chi_{[0,c]}(k+k_{1}) + \chi_{[0,c]}(|k-k_{1}|) - 2\chi_{[0,c]}(\max\{k,k_{1}\})] dk dk_{1}.$$

Set  $K(k, k_1) = \chi_{[0,c]}(k + k_1) + \chi_{[0,c]}(|k - k_1|) - 2\chi_{[0,c]}(\max\{k, k_1\})$ . There are seven cases as follows:

- (i) Assume  $k + k_1 \le c$ ; then we have  $\chi_{[0,c]}(k + k_1) = 1$ ,  $\chi_{[0,c]}(|k k_1|) = 1$  and  $\chi_{[0,c]}(\max\{k,k_1\}) = 1$  which implies that  $K(k,k_1) = 0$ .
- (ii) Assume that  $k + k_1 > c$  but  $k \le c$  and  $k_1 \le c$ . Then we have  $\chi_{[0,c]}(k+k_1) = 0$ ,  $\chi_{[0,c]}(|k-k_1|) = 1$ ,  $\chi_{[0,c]}(\max\{k,k_1\}) = 1$ , and so  $K(k,k_1) = -1$ .
- (iii) Now let  $k + k_1 > c$ ,  $k \le c$  but  $k_1 > c$ ; then  $\chi_{[0,c]}(k+k_1) = 0$ ,  $\chi_{[0,c]}(|k-k_1|) = 1$ , and  $\chi_{[0,c]}(\max\{k,k_1\}) = 0$ , giving  $K(k,k_1) = 1$ .
- (iv) Assume  $k+k_1 > c$ , with k > c and  $k_1 \le c$  and  $|k-k_1| > c$ ; then  $\chi_{[0,c]}(k+k_1) = 0$ ,  $\chi_{[0,c]}(|k-k_1|) = 0$ ,  $\chi_{[0,c]}(\max\{k,k_1\}) = 0$ , leaving  $K(k,k_1) = 0$ .
- (v) Assume  $k + k_1 > c$ , with k > c and  $k_1 \le c$  and  $|k k_1| \le c$ ; then  $\chi_{[0,c]}(k + k_1) = 0$ ,  $\chi_{[0,c]}(|k k_1|) = 1$ ,  $\chi_{[0,c]}(\max\{k,k_1\}) = 0$ , leaving  $K(k,k_1) = 1$ .
- (vi) Lastly, set  $k + k_1 > c$ , k > c,  $k_1 > c$ , and  $|k k_1| > c$ ; then  $\chi_{[0,c]}(k + k_1) = 0$ ,  $\chi_{[0,c]}(|k k_1|) = 0$ , and  $\chi_{[0,c]}(\max\{k,k_1\}) = 0$ , resulting in  $K(k,k_1) = 0$ .
- (vii) Lastly, set  $k + k_1 > c$ , k > c,  $k_1 > c$ , and  $|k k_1| \le c$ ; then  $\chi_{[0,c]}(k + k_1) = 0$ ,  $\chi_{[0,c]}(|k k_1|) = 1$ , and  $\chi_{[0,c]}(\max\{k,k_1\}) = 0$ , resulting in  $K(k,k_1) = 1$ .

Applying these computations to (2.6) and after taking the derivative as done for (2.3), we have

which gives

(2.8) 
$$\partial_t f(t,c) = -2\partial_c \int_0^c \int_0^c a(k,k_1) f(k) f(k_1) \chi \{c < k + k_1\} dk_1 dk + \partial_c \int_0^\infty \int_0^\infty a(k,k_1) f(k) f(k_1) k_1 \chi \{c < k + k_1\} dk dk_1,$$

yielding 
$$(2.4)$$
.

With the identity (2.4) at hand, we now derive an FVS with which to solve it. Note that with (2.4), we only need to truncate a single term, while with the original formula (1.16), we are required to truncate three terms.

**3. Finite volume scheme.** We give a discretization for the frequency domain for  $k \in [0, R]$ . Let  $i \in \{1, 2, ..., M\} = I_h^M$ , with the maximum stepsize  $h \in (0, 1)$  fixed. We define the set of cells  $\mathcal{K} = \bigcup_{i \in I_h^M} K_i = [0, R]$  to be the discretization of the wavenumber domain into M cells. Let

$$K_i = [k_{i-1/2}, k_{i+1/2})_{i \in I_h^M}, \quad \{k_i\}_{i \in I_h^M} = \frac{k_{i+1/2} + k_{i-1/2}}{2}, \quad \{h_i\}_{i \in I_h^M} = k_{i+1/2} - k_{i-1/2}$$

define the cells, pivots, and stepsize, respectively, with the boundary nodes  $k_{1/2}=0$  and  $k_{M+1/2}=R$ . Note that the discretization does not require a uniform grid but does restrict the stepsize in each cell  $K_i$  so that  $h_i \leq h$ . In practice, it can be useful to drop the restriction that  $h \in (0,1)$ , especially when using a nonuniform grid, though we leave it here to simplify the analysis. The set  $T_N = \{0, \ldots, T\}$  with N+1 nodes, where T is the maximum time, is the discretization of the time domain. We fix the time step to be  $\Delta t = \frac{T}{N}$  and denote  $t_n = \Delta t \cdot n$  for  $n \in \{0, \ldots, N\}$ . We approximate (2.4) with

(3.1) 
$$g^{n+1}(k_i) = g^n(k_i) + \lambda_i \left( Q_{i+1/2}^n \left[ \frac{g}{k} \right] - Q_{i-1/2}^n \left[ \frac{g}{k} \right] \right),$$

where  $\lambda_i = \frac{k_i \Delta t}{h_i}$ , and

$$\begin{split} Q_{i+1/2}^{n} \Big[ \frac{g}{k} \Big] - Q_{i-1/2}^{n} \Big[ \frac{g}{k} \Big] &= -2 \Bigg( Q_{1,i+1/2}^{n} \Big[ \frac{g}{k} \Big] - Q_{1,i-1/2}^{n} \Big[ \frac{g}{k} \Big] \Bigg) \\ &+ \Bigg( Q_{2,i+1/2}^{n} \Big[ \frac{g}{k} \Big] - Q_{2,i-1/2}^{n} \Big[ \frac{g}{k} \Big] \Bigg), \end{split}$$

with

$$(3.2) \quad Q_{1,i+1/2}^n \left[ \frac{g}{k} \right] = \sum_{m=1}^i h_m \frac{g^n(k_m)}{k_m} \left( \sum_{j=1}^i h_j \frac{g^n(k_j)}{k_j} a(k_m, k_j) \chi \left\{ k_{i+1/2} < k_m + k_j \right\} \right),$$

$$(3.3) \quad Q_{2,i+1/2}^n \left[ \frac{g}{k} \right] = \sum_{m=1}^M h_m \frac{g^n(k_m)}{k_m} \left( \sum_{j=1}^M h_j \frac{g^n(k_j)}{k_j} a(k_m,k_j) \chi \left\{ k_{i+1/2} < k_m + k_j \right\} \right),$$

where we have used the midpoint rule to approximate the integrals in (2.4), and we choose an explicit time stepping method.

We will be interested in computing the moments of our solution. We approximate the  $\ell$ th moment,  $\mathcal{M}^{\ell}(t_n)$ , by

(3.4) 
$$\mathcal{M}^{\ell}(t_n) = \sum_{i=1}^{M} h_i g^n(k_i) k_i^{\ell},$$

with  $\ell \in \mathbb{N}$ .

The initial condition  $g_0(k)$  is approximated by

$$g^{0}(k_{i}) = \frac{1}{h_{i}} \int_{k_{i-1/2}}^{k_{i+1/2}} g_{0}(k) dk \approx g_{0}(k_{i}),$$

again employing the midpoint rule. We have that  $g^0(k_i) \geq 0$  for all  $i \in \{1, ..., M\}$  since  $g_0(k) \geq 0$  for all  $k \in [0, R]$  by assumption. To ease notation in the proof of the following proposition, we write  $g_i^n$  for  $g^n(k_i)$  and the negative flux as

$$\left[Q_{i}^{n}\right]^{\mp} = Q_{i-1/2}^{n} \left[\frac{g}{k}\right] - Q_{i+1/2}^{n} \left[\frac{g}{k}\right],$$

so that the forward Euler scheme becomes  $g_i^{n+1} = g_i^n - \lambda_i [Q_i^n]^{\mp}$ . Let us analyze the collision operator (3.5). For the moment, we leave (3.5) in continuous form but will apply the same midpoint approximation when appropriate. Then we have

$$[Q_{i}^{n}]^{\mp} = \left(2\int_{0}^{k_{i+1/2}} \int_{0}^{k_{i+1/2}} g_{1}^{n} g_{2}^{n} (k_{1}k_{2})^{\gamma/2-1} \chi \left\{k_{i+1/2} < k_{1} + k_{1}\right\} dk_{2} dk_{1} \right)$$

$$- \int_{0}^{R} \int_{0}^{R} g_{1}^{n} g_{2}^{n} (k_{1}k_{2})^{\gamma/2-1} \chi \left\{k_{i+1/2} < k_{1} + k_{1}\right\} dk_{2} dk_{1} \right)$$

$$- \left(2\int_{0}^{k_{i-1/2}} \int_{0}^{k_{i-1/2}} g_{1}^{n} g_{2}^{n} (k_{1}k_{2})^{\gamma/2-1} \chi \left\{k_{i-1/2} < k_{1} + k_{1}\right\} dk_{2} dk_{1} \right)$$

$$- \int_{0}^{R} \int_{0}^{R} g_{1}^{n} g_{2}^{n} (k_{1}k_{2})^{\gamma/2-1} \chi \left\{k_{i-1/2} < k_{1} + k_{1}\right\} dk_{2} dk_{1} \right) = (I - II) - (III - IV),$$

with  $g_i^n = g^n(k_i)$  for i = 1, 2. We may decompose the integrals above so that

$$I = 2 \int_{0}^{k_{i-1/2}} \int_{0}^{k_{i-1/2}} g_{1}^{n} g_{2}^{n} (k_{1}k_{2})^{\gamma/2-1} \chi \Big\{ k_{i+1/2} < k_{1} + k_{1} \Big\} dk_{2} dk_{1}$$

$$+ 2 \int_{0}^{k_{i-1/2}} \int_{k_{i-1/2}}^{k_{i+1/2}} g_{1}^{n} g_{2}^{n} (k_{1}k_{2})^{\gamma/2-1} \chi \Big\{ k_{i+1/2} < k_{1} + k_{1} \Big\} dk_{2} dk_{1}$$

$$+ 2 \int_{k_{i-1/2}}^{k_{i+1/2}} \int_{0}^{k_{i-1/2}} g_{1}^{n} g_{2}^{n} (k_{1}k_{2})^{\gamma/2-1} \chi \Big\{ k_{i+1/2} < k_{1} + k_{1} \Big\} dk_{2} dk_{1}$$

$$+ 2 \int_{k_{i-1/2}}^{k_{i+1/2}} \int_{k_{i-1/2}}^{k_{i+1/2}} g_{1}^{n} g_{2}^{n} (k_{1}k_{2})^{\gamma/2-1} \chi \Big\{ k_{i+1/2} < k_{1} + k_{1} \Big\} dk_{2} dk_{1}$$

$$= 2 \int_{0}^{k_{i-1/2}} \int_{0}^{k_{i-1/2}} g_{1}^{n} g_{2}^{n} (k_{1}k_{2})^{\gamma/2-1} \chi \Big\{ k_{i+1/2} < k_{1} + k_{1} \Big\} dk_{2} dk_{1}$$

$$+ 4 \int_{k_{i-1/2}}^{k_{i+1/2}} \int_{0}^{k_{i-1/2}} g_{1}^{n} g_{2}^{n} (k_{1}k_{2})^{\gamma/2-1} \chi \Big\{ k_{i+1/2} < k_{1} + k_{1} \Big\} dk_{2} dk_{1}$$

$$+ 2 \int_{k_{i-1/2}}^{k_{i+1/2}} \int_{k_{i-1/2}}^{k_{i+1/2}} g_{1}^{n} g_{2}^{n} (k_{1}k_{2})^{\gamma/2-1} \chi \Big\{ k_{i+1/2} < k_{1} + k_{1} \Big\} dk_{2} dk_{1},$$

and similar decompositions may be performed on II, III, and IV, which, leaving out the  $g_1^n g_2^n (k_1 k_2)^{\gamma/2-1}$  integrands to simplify the expressions, gives

$$\begin{aligned} \left[Q_{i}^{n}\right]^{\mp} &= 2\int_{0}^{k_{i-1/2}} \int_{0}^{k_{i-1/2}} \left(\chi\left\{k_{i+1/2} < k_{1} + k_{1}\right\} - \chi\left\{k_{i-1/2} < k_{1} + k_{1}\right\}\right) \mathrm{d}k_{2} \mathrm{d}k_{1} \\ &+ \int_{0}^{R} \int_{0}^{R} \left(\chi\left\{k_{i-1/2} < k_{1} + k_{1}\right\} - \chi\left\{k_{i+1/2} < k_{1} + k_{1}\right\}\right) \mathrm{d}k_{2} \mathrm{d}k_{1} \\ &+ 4\int_{k_{i-1/2}}^{k_{i+1/2}} \int_{0}^{k_{i-1/2}} \chi\left\{k_{i+1/2} < k_{1} + k_{1}\right\} \mathrm{d}k_{2} \mathrm{d}k_{1} \\ &+ 2\int_{k_{i-1/2}}^{k_{i+1/2}} \int_{k_{i-1/2}}^{k_{i+1/2}} \chi\left\{k_{i+1/2} < k_{1} + k_{1}\right\} \mathrm{d}k_{2} \mathrm{d}k_{1}, \\ &= 2\int_{0}^{k_{i-1/2}} \int_{0}^{k_{i-1/2}} \chi\left\{k_{i-1/2} < k_{1} + k_{1} \le k_{i+1/2}\right\} \mathrm{d}k_{2} \mathrm{d}k_{1} \\ &+ \int_{0}^{R} \int_{0}^{R} \chi\left\{k_{i-1/2} < k_{1} + k_{1} \le k_{i+1/2}\right\} \mathrm{d}k_{2} \mathrm{d}k_{1} \end{aligned}$$

$$+ 4 \int_{k_{i-1/2}}^{k_{i+1/2}} \int_{0}^{k_{i-1/2}} \chi \left\{ k_{i+1/2} < k_1 + k_1 \right\} dk_2 dk_1$$

$$+ 2 \int_{k_{i-1/2}}^{k_{i+1/2}} \int_{k_{i-1/2}}^{k_{i+1/2}} \chi \left\{ k_{i+1/2} < k_1 + k_1 \right\} dk_2 dk_1.$$

At this point, we apply the midpoint rule to approximate the integrals which, after making use of the characteristic functions, simplifies the above to

$$(3.9) \qquad \left[Q_i^n\right]^{\mp} \approx 2g_i^n k_i^{\gamma/2-1} h_i \left(\sum_{j=1}^i g_j^n k_j^{\gamma/2-1} h_j + \sum_{j=1}^{i-1} g_j^n k_j^{\gamma/2-1} h_j\right) - \sum_{j=1}^{i-1} g_j^n g_{i-j}^n (k_j k_{i-j})^{\gamma/2-1} h_j h_{i-j}.$$

In what follows, we will abuse notation slightly and write  $[Q_i^n]^{\mp}$  when we mean its midpoint approximation above.

We are now in position to state the following sufficient stability condition for the time step.

Proposition 3.1. If the time step  $\Delta t$  satisfies

(3.10) 
$$\Delta t R^{\gamma+1} \|g^0\|_{L^{\infty}(0,R)} \le \frac{\gamma}{16} \min_{i \in I_h^M} h_i,$$

then for all  $n \ge 0$  and  $i \in I_h^M$  we have  $g_i^n \ge 0$ , and further,

$$||g^{n+1}||_{L^{\infty}(0,R)} \le C(\gamma)||g^n||_{L^{\infty}(0,R)}$$

with  $C(\gamma) \in \left[\frac{15}{16}, 1\right]$  so that finally,

(3.11) 
$$||g^n||_{L^{\infty}(0,R)} \le ||g^0||_{L^{\infty}(0,R)}$$

for all  $n \ge 0$ .

*Proof.* Assume  $R \gg 1$ . We will proceed by induction. Starting from the forward Euler scheme and using  $[Q_i^0]^{\mp}$  as computed above, we obtain

$$(3.12) g_i^1 = g_i^0 \left( 1/2 - \lambda_i \left( 2k_i^{\gamma/2-1} h_i \left[ \sum_{j=1}^i g_j^0 k_j^{\gamma/2-1} h_j + \sum_{j=1}^{i-1} g_j^0 k_j^{\gamma/2-1} h_j \right] \right) \right)$$

$$+ \frac{1}{2} g_i^0 + \lambda_i \sum_{j=1}^{i-1} g_j^0 g_{i-j}^0 (k_j k_{i-j})^{\gamma/2-1} h_j h_{i-j} = \varphi_i^0(g) + \zeta_i^0(g).$$

Given  $g_i^0 \ge 0$ ,  $\zeta_i^0(g)$  is clearly positive. Then, to conclude that  $g_i^1 \ge 0$ , it is sufficient to have  $\varphi_i^0(g) \ge 0$  or, equivalently,

$$(3.13) \Delta t \frac{k_i}{h_i} \left( 2k_i^{\gamma/2-1} h_i \left[ \sum_{i=1}^i g_j^0 k_j^{\gamma/2-1} h_j + \sum_{i=1}^{i-1} g_j^0 k_j^{\gamma/2-1} h_j \right] \right) \le \frac{1}{2}.$$

To this end, note that

$$k_i \left( 2k_i^{\gamma/2-1} h_i \left[ \sum_{j=1}^i g_j^0 k_j^{\gamma/2-1} h_j + \sum_{j=1}^{i-1} g_j^0 k_j^{\gamma/2-1} h_j \right] \right)$$

$$(3.14) \leq 4k_i^{\gamma/2} \|g^0\|_{L^{\infty}(0,R)} \|k^{\gamma/2-1}\|_{L^1(0,R)} \leq \frac{8}{\gamma} R^{\gamma+1} \|g^0\|_{L^{\infty}(0,R)}.$$

For now, we provide a provisional stability condition on  $\Delta t$  so that

(3.15) 
$$\Delta t R^{\gamma+1} \max_{\ell \le n} \{ \|g^{\ell}\|_{L^{\infty}(0,R)} \} \le \frac{\gamma}{16} \min_{i \in I_h^M} h_i,$$

which will be seen to be equivalent to the condition (3.10) by the end of the proof. Thus, with (3.15) setting n = 0 we have that  $\varphi_i^0(g)$  is positive. Now, assuming  $g_i^n \ge 0$ , we proceed in the same fashion. The steps are identical except that now we have the condition that

(3.16) 
$$\Delta t R^{\gamma+1} \|g^n\|_{L^{\infty}(0,R)} \le \frac{\gamma}{16} \min_{i \in I_h^M} h_i,$$

which again is satisfied by the provisional assumption on  $\Delta t$ , and we have by induction that  $g_i^{n+1} \geq 0$  as desired.

To show stability, let us consider  $\zeta_i^n(g)$  and give estimates for its second term. To this end, note that

(3.17) 
$$\frac{k_i}{h_i} \sum_{j=1}^{i-1} g_j^n g_{i-j}^n (k_j k_{i-j})^{\gamma/2-1} h_j h_{i-j} \leq k_i \|g^n\|_{L^{\infty}(0,R)}^2 \sum_{j=1}^M k_j^{\gamma-1} h_j \\
\leq \frac{k_i}{\gamma} R^{\gamma} \|g^n\|_{L^{\infty}(0,R)}^2 \leq \frac{1}{\gamma} R^{\gamma+1} \|g^n\|_{L^{\infty}(0,R)}^2,$$

where the rearrangement inequality was used in the second line. Then, using (3.15), we obtain

(3.18) 
$$\Delta t \frac{k_i}{h_i} \sum_{j=1}^{i-1} g_j^n g_{i-j}^n (k_j k_{i-j})^{\gamma/2-1} h_j h_{i-j} \le \frac{1}{16} \|g^n\|_{L^{\infty}(0,R)}.$$

Once again, using the assumption (3.15) we see that

$$(3.19) g_i^{n+1} = \varphi_i^n(g) + \zeta_i^n(g) \le g_i^n \left(\frac{8-\gamma}{16}\right) + \frac{1}{2}g_i^n + \frac{1}{16}\|g^n\|_{L^{\infty}(0,R)},$$

which implies that

We see that for  $\gamma \in [1,2]$  we have  $C(\gamma) \in [\frac{15}{16},1]$  and thus

(3.21) 
$$||g^{n+1}||_{L^{\infty}(0,R)} \le ||g^{0}||_{L^{\infty}(0,R)},$$

which gives the equivalence of condition (3.15) with (3.10).

In the following section we provide numerical results for several initial conditions, which give evidence for the dependence of the timesteps on the initial condition and truncation parameter as demonstrated above.

**4. Numerical tests.** As mentioned above, the KZ spectrum is not expected in our equation due to the absence of forcing and dissipation. Our numerical tests are therefore only designed to verify the blow-up phenomenon first proved in [39] and to confirm the energy cascade growth rate bound  $\mathcal{O}(1/\sqrt{t})$  obtained in the same paper. To verify this, in any finite interval of the wavenumber domain, we should see the total energy  $\mathcal{E}$  or, equivalently, the zeroth moment of g(t,k), decaying like  $\mathcal{O}(\frac{1}{\sqrt{t}})$  in the interval. As (1.4)-(1.5)-(1.6)-(1.7) is equivalent to (1.8), our numerical tests will focus on verifying (1.8).

All tests were performed on a uniform grid, with h=0.5 in the first two tests and h=0.1 in the last two. We solve the 3-wave equation via (2.4) for four different initial conditions. For each initial condition, we either vary the truncation parameter, R, in (1.8), and hold the degree of the collision kernel,  $\gamma$ , fixed, or we vary  $\gamma$  with R kept at a fixed value. Specifically, for the first two initial conditions, we run tests for R=50,100,200 with  $\gamma=2$  fixed or  $\gamma=\frac{3}{2},\frac{9}{5},2$  with R=100 fixed. In the last two cases, we do something similar and again run tests with  $\gamma=2$  fixed but set R=25,50,80, then fix R=50, and let  $\gamma=\frac{3}{2},\frac{9}{5},2$ . We provide an approximation of the convergence rate for the first initial condition by a comparison of approximated solutions over successively refined grids. In all solutions presented, we use a second-order Runge–Kutta scheme to integrate in time.

The first few moments of the energy, g(t,k), are then computed for each set of parameters. We find our numerical experiments to be in good agreement with [39]. We note that, as with explicit methods for the Smoluchowski equation, the CFL condition can be very restrictive if one wants to maintain positivity (see [25]). Similarly to schemes for other types of kinetic equations, maintaining positivity of the numerical solutions is also an important issue in our scheme.

We provide a condition in Proposition 3.1 that guarantees the positivity of the solutions. Under this condition, the positivity can be preserved when we choose  $\Delta t$  sufficiently small.

We observe that the choice of  $\Delta t$  depends on the initial data and the size of the truncated interval. For example, in Test 1 we set  $\Delta t = 0.05$ , and in Test 2 we set  $\Delta t = 0.005$ , though we perform computations with the same truncation parameter. Also, in Tests 3 and 4, as we increase the truncation parameter from R = 50 to R = 80, we must drop the time step from  $\Delta t = 0.0004$  to  $\Delta t = 0.00025$ , respectively.

We believe that common positivity preserving techniques like those developed in [19, 20, 21] could potentially be a solution to handling this instability issue.

**4.1.** Test 1. Here we choose our initial condition to be

(4.1) 
$$g_0(k) = 1.26157e^{-50(k-1.5)^2},$$

with  $\Delta t = 0.05$  for  $t \in [0, T]$ , T = 10000, over a uniform grid, as mentioned previously, with h = 0.5. The initial condition and final state, g(T, k), are plotted in Figures 4.1a and 4.1b, respectively, for  $\gamma = 2$ . The theory developed in [39], in which it was proved that as t tends to  $\infty$ , the energy g(t, k) converges to a delta function  $\mathcal{E}\delta_{\{k=\infty\}}$ , applies for  $\gamma > 1$ . Moreover, due to (1.8), the energy on any finite interval also goes to 0:

(4.2) 
$$\lim_{t \to \infty} g(t, k) \chi_{[0, R]}(k) = 0.$$

Both Figures 4.1a and 4.1b indeed give strong evidence for the theoretical result (4.2) proved in [39].

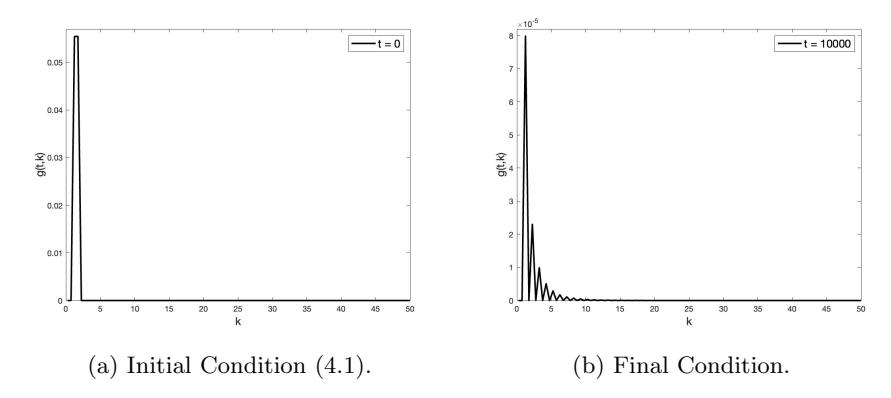


Fig. 4.1. Test Case 1.

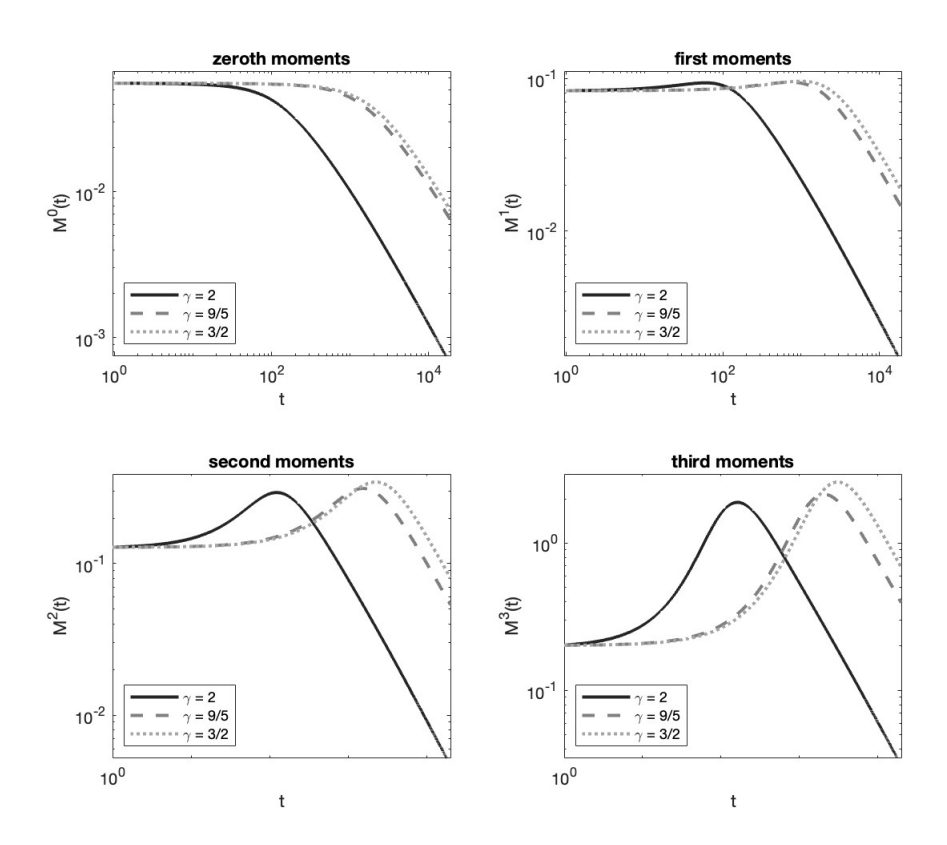


Fig. 4.2. Here, we fix R=100 and compute the moments of the energy as a function of time for  $\gamma=3/2,9/5,~$  and 2 for initial condition (4.1).

The first four moments of the energy are shown in Figure 4.2 for  $\gamma = \frac{3}{2}, \frac{9}{5}, 2$  and  $k \in [0, 100]$ . The numerical results in Figure 4.2 show that higher moments of g also decay to 0, due to (4.2). We also see that the onset of decay happens later for smaller degree  $\gamma$ . For the zeroth moment, the curve corresponding to  $\gamma = 2$  is below the curve

for  $\gamma=3/2$  and the curve for  $\gamma=9/5$ . However, for the higher order moments, an interesting phenomenon occurs. The  $\gamma=3/2$  curve has a big jump when t is around 10–40, and it lies above the other moments from that time on, while the  $\gamma=2$  curve is still below the  $\gamma=9/5$  curve at longer times. While (4.2) can be used to predict what happens in Figures 4.1, 4.2 indeed needs a different theoretical explanation, which should be an interesting subject of analysis in a follow-up paper.

We then investigate the moments for increasing values of the truncation parameter. The first four moments of g(t,k) are plotted in Figure 4.3, with  $\gamma=2$  fixed. For this initial condition, as might be expected, increasing the truncation parameter seems to have a negligible effect on the higher moments. For the other initial conditions in the test cases that follow, the difference is more distinguishable. When we are able to make a distinction, the decay (4.2) seems to be slower for larger values of the truncation parameter R, though the rate of cascade is unaffected. Moreover, when the initial condition spreads the energy across the interval, larger truncation parameters result in larger amounts of energy initially, as one might expect, but again the cascade rate is independent of the truncation value in these cases. This observation is consistent with the findings of [39] and can be understood as follows. As the energy moves away from the zero frequency k=0 and goes to the frequency  $k=\infty$  as time evolves, the chance of having some energy in a finite interval  $k \in [0,R]$  increases when R increases.

To test convergence without an exact solution, we provide two experimental order of convergence (EOC) tests. First, we compare stepsizes h, h/2, and h/4 for R=50 and  $\gamma=2$ . Here we run the simulation for  $t\in[0,T_{EOC}]$  with  $T_{EOC}=25$  and  $\Delta t=0.0125$  for every choice of h. The approximate order of convergence, p, is given by [26] as

$$(4.3) p \approx \log_2 \left( \frac{\|g_h - g_{h/4}\|_{L^1}}{\|g_{h/2} - g_{h/4}\|_{L^1}} - 1 \right).$$

The coarser solutions are interpolated using the MATLAB built-in piecewise cubic Hermite interpolating polynomial (pchip) interpolator. Table 4.1 summarizes the approximation of p for each h at  $t_{max} = \arg \max \|g_h - g_{h/4}\|_{L^1}$ .

Next, we approximate p by comparison with a fine grid solution,  $g_{h^*}$ , with  $h^* = \frac{1}{80}$  and  $\Delta t$  as before. Then we approximate p with the ratio [26]

$$(4.4) R_h(t) = \left(\frac{\|g_h - g_{h^*}\|_{L^1(0,R)}}{\|g_{h/2} - g_{h^*}\|_{L^1(0,R)}}\right).$$

Then, the EOC is given by  $p \approx \log_2\{R_h(T_{EOC})\}$ . The results for h = 0.2, h = 0.1 are summarized in Table 4.2.

A log-log plot of the errors is provided in Figure 4.4. The verification of these experiments requires further analysis, which is the subject of a forthcoming work.

We test the decay rate of the total energy in  $[0, \infty)$  obtained in [39] in Figures 4.5a and 4.5b. We give a log-log plot of the zeroth moment of g(t, k) for varying truncation parameter with  $\gamma = 2$ , and with fixed truncation parameter R = 200 with varying

Table 4.1 Approximation of p with formula (4.3) for various h values.

$\overline{h}$	0.4	0.3	0.2
p	2.5777	2.6071	2.6392

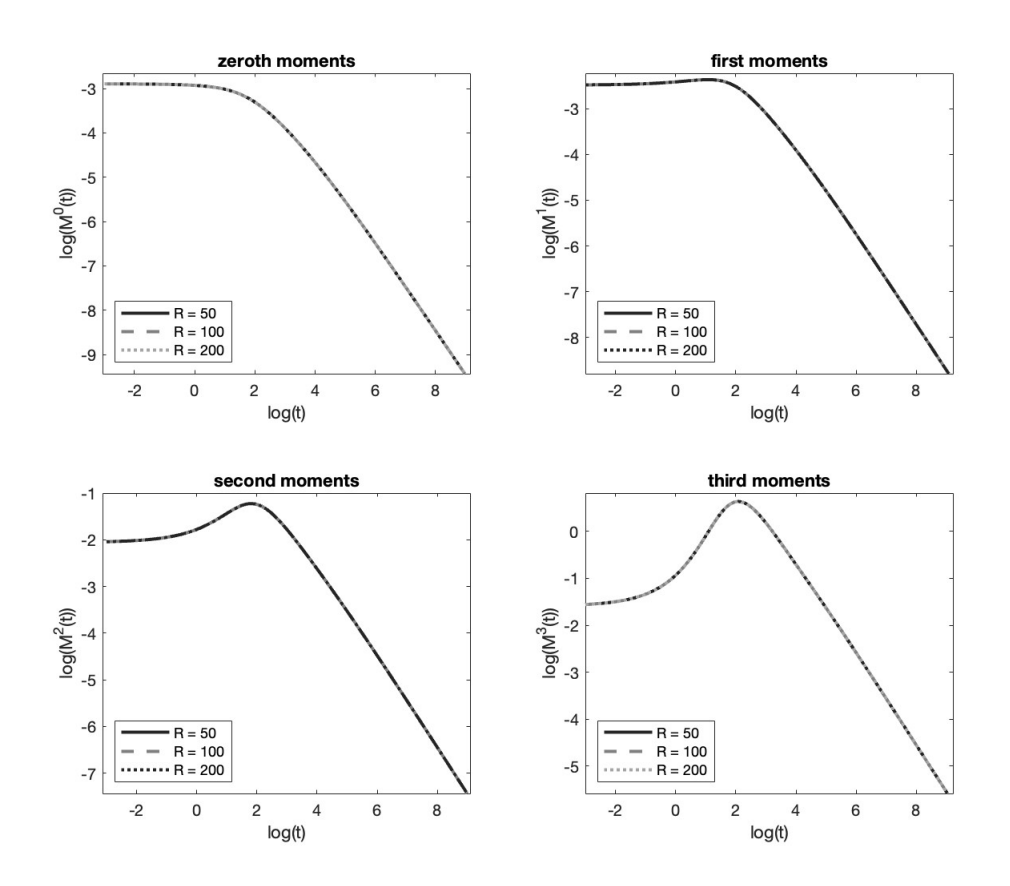


Fig. 4.3. For  $\gamma=2$  fixed, we compute the moments of the energy with initial condition (4.1) for truncation parameters R=50,100,200.

Table 4.2 Approximation of p with formula (4.3) for various h values.

0.1

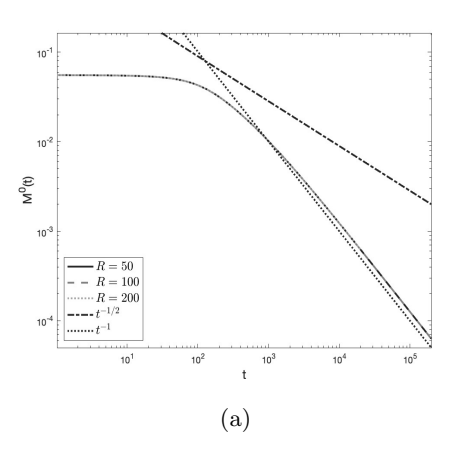
2.5288

0.2

2.0118

	h=0.2
,	h=0.1
	h=0.05
_	~
£ 4	``.
9	
8/2	-
(19, -9, -9, -9)	*******
ъ́ "	***************************************
4-	
-4	
	******

Fig. 4.4. Log-log plot of the error between coarse and fine grid solutions.



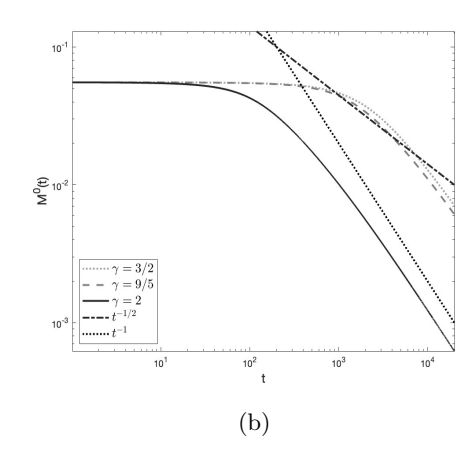


Fig. 4.5. (a) Rate of decay of the total energy, corresponding to initial condition (4.1) with degree  $\gamma=2$ , allowing R to vary. The theoretical cascade rate is shown for comparison. (b) Rate of decay of the total energy corresponding to the initial condition (4.1), with theoretical cascade rate plotted for comparison.

degree against the theoretical decay rate of the total energy in  $[0, \infty)$ . In [39], it was shown that the decay rate can be bounded by  $\mathcal{O}\left(\frac{1}{\sqrt{t}}\right)$  (see (1.8)), which has very good agreement with the numerical results, where the slope of the decay rate curve in the long time limit is quite below the slope of the line corresponding to  $\frac{1}{\sqrt{t}}$ . We also compare with a rate like  $\mathcal{O}\left(\frac{1}{t}\right)$ . Here, and for the other initial conditions we consider, it would appear that the rate is like  $\mathcal{O}\left(\frac{1}{t^s}\right)$ , with  $s \in [1/2, 1]$ , depending on the degree and the initial condition. Confirmation of this observation requires further analysis.

We present below some preliminary observations of the so-called transient spectra, which are predicted to occur for finite capacity systems. These spectra are different from the KZ spectra discussed above and cannot be estimated from dimensional arguments or via applying Zakharov transformations in the 3-wave kinetic equation. Briefly, the transient spectra should occur just before the singular behavior time  $t_1^*$ , and the solution should have the form  $f_{trans}(t,k) \approx C_{trans}k^{-a}$  for a > 0, where, importantly,  $a \neq \kappa$  for  $\kappa$  the exponent of the KZ solution. In Figure 4.6, we give a log-log plot of the initial condition and the solution just before the cascade process begins. We draw a comparative line through this snapshot in time of the solution. Lines corresponding to the KZ spectra for capillary and acoustic waves are also shown for comparison. To rigorously compute a, one must solve a nonlinear eigenvalue problem as in [9]. However, as discussed above, solving such a nonlinear eigenvalue problem is a difficult task: in [9], a hypothesis is imposed on the evolution of the solution. The solution is assumed to grow linearly in time (1.13), and additional hypotheses are also imposed to treat the singularities of the integral (1.12). While these hypotheses remain interesting mathematical questions to be verified, we assume that the nonlinear interactions are solely responsible for the transfer of energy in our work. We provide Figure 4.6 as preliminary evidence that the solution seems to give a cascade behavior consistent with the predicted transient spectra, though further rigorous analysis is required for verification. To reiterate, our main concerns in the present article are to study the behavior of g(t,k) after the first blow-up time and to show the existence of the multiple blow-up time phenomenon  $t_1^* < \cdots < t_n^* < \cdots$ , while the transient

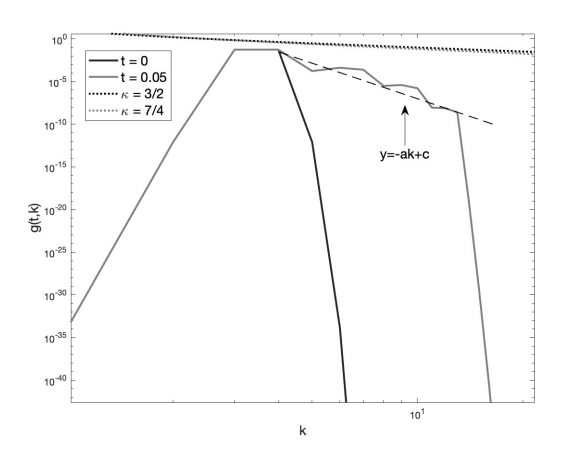


Fig. 4.6. Transient cascade.

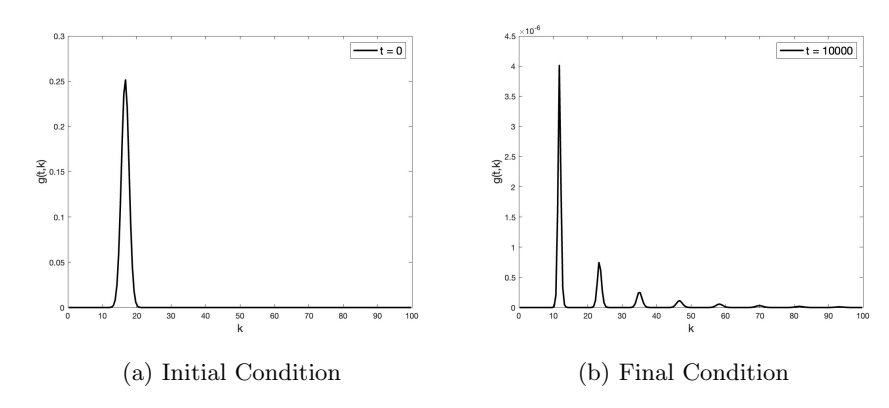


Fig. 4.7. Test case 2.

cascade occurs just prior to the first blow-up time  $t_1^*$ . Finding self-similar profiles for the solutions before the *n*th blow-up times, similarly to those given in [2, 9, 38], is nontrivial and will be the subject of future work.

4.2. Test 2. We next choose a Gaussian further away from the origin

(4.5) 
$$g_0(k) = (5\pi)^{-1/2} e^{-(k-50/3)^2/2.5}$$

as our initial condition. Solutions are computed up to T=10000 with  $\Delta t=0.005$  and h=0.5. The initial condition and final state can be seen in Figures 4.7a and 4.7b, respectively. This test is designed based on Test 1, as we are curious to see what happens if we move the Gaussian away from zero.

In Figures 4.7a and 4.7b we see that the energy is pushed slightly toward the origin at some  $T_s \in [0,T)$  to k=11.75, away from its initial concentration at k=16.667 at t=0. From this time  $T_s$  onward, the  $L^{\infty}$  norm of  $\|g(t,k)\chi_{[0,R]}(k)\|_{L^{\infty}}$  decreases to  $4.01 \times 10^{-5}$  for t=10000, maintaining its concentration at k=11.75. This indicates that the energy cascade phenomenon does occur and happens in a very special way. An analysis then needs to be done to explain this long time behavior of the solution.

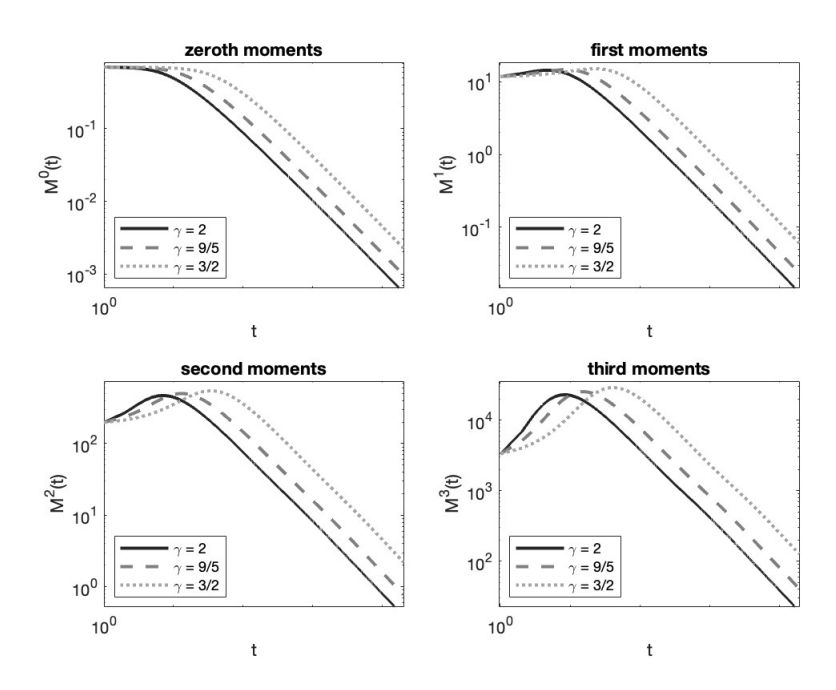


Fig. 4.8. Here, we fix R = 100 and compute the moments of the energy as a function of time for  $\gamma = 3/2, 9/5, 2$  with initial condition (4.1).

In Figure 4.8, we give results for the computation of the first few moments of the energy when allowing the degree to vary while holding the truncation value fixed. We notice a behavior similar to that in the previous test case.

The moment calculations are performed with  $\gamma=2$  fixed and varying truncation parameter. The results are plotted in Figure 4.9. In contrast to Figure 4.3, the difference in moments is more distinguishable. However, as already mentioned, this is consistent with the previous analysis in [39], being that the chance of finding energy in a larger frequency interval is higher.

The theoretical decay rate is compared with the decay of total energy for all considered values of  $\gamma$  and R=100 in Figure 4.10b. As in Test 1, the numerical results have a good agreement with the theoretical findings of [39]. It appears that the decay is more like  $\mathcal{O}(\frac{1}{t})$ , which is bounded by  $\mathcal{O}(\frac{1}{\sqrt{t}})$  as shown in (1.8). We also compare the theoretical cascade rate to the decay of total energy for each interval considered in Figure 4.10a.

We see that increasing the truncation parameter has no influence on the cascade rate and blow-up times, which is consistent with the theory found in [39]. We notice that here and in the previous test case, there is also not a distinguishable difference (if any) in the amount of energy contained in the intervals after varying the truncation parameter, which will contrast with the next two test cases, where much more energy is available initially.

As in the previous test, we provide possible evidence for the transient spectra and compare them with the known KZ spectra of the relevant systems. The results are shown in Figure 4.11.

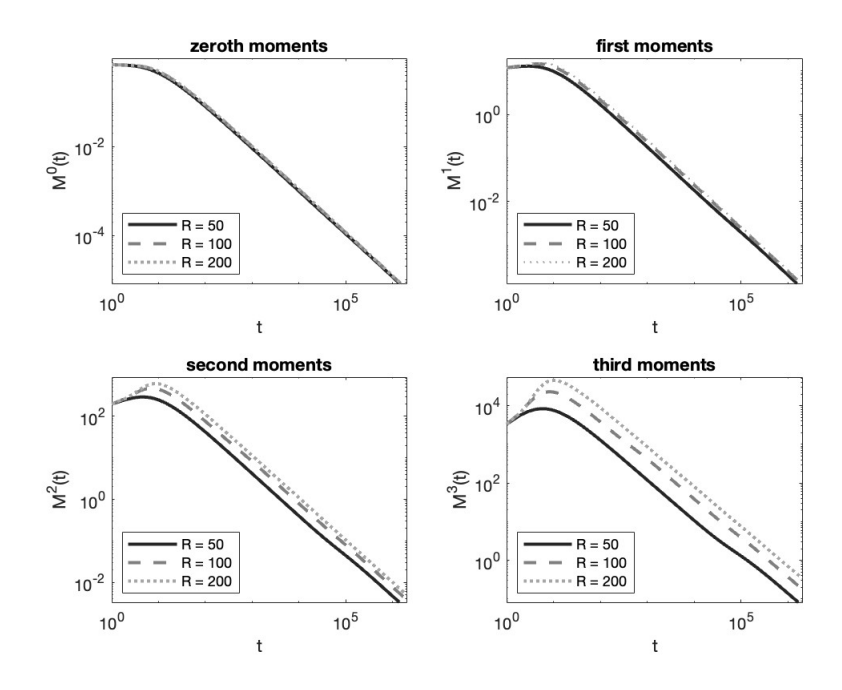


Fig. 4.9. Moments of g(t,k) with initial condition (4.5), fixed degree  $\gamma = 2$ , and varying truncation parameter.

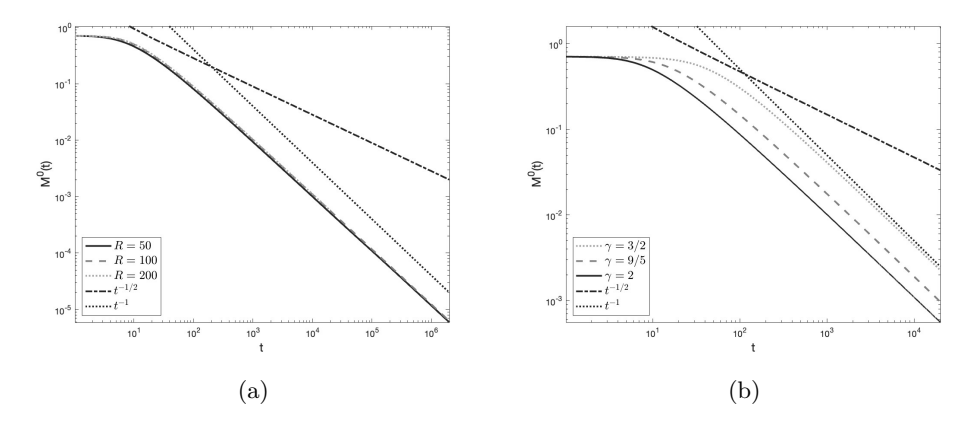


FIG. 4.10. (a) Rate of decay of the total energy with varying truncation parameter corresponding to the initial condition shown in Figure 4.7a. (b) Rate of decay of the total energy corresponding to the initial condition shown in Figure 4.7a with varying degree and theoretical rate plotted for comparison.

## **4.3.** Test **3.** Here, we consider initial data given by

(4.6) 
$$g_0(k) = \begin{cases} 1 & k \in [2n\pi, (2n+1)\pi] \\ 0 & k \in ((2n+1)\pi, 2(n+1)\pi) \end{cases} \text{ for } n = 0, 1, 3, 5, \dots$$

and perform a test for  $t \in [0, T]$  for T = 100 and  $\Delta t = 0.0004$  when R = 25 and R = 50 and  $\Delta t = 0.00025$  for R = 80. The frequency step is h = 0.1 for each interval [0, R] considered.

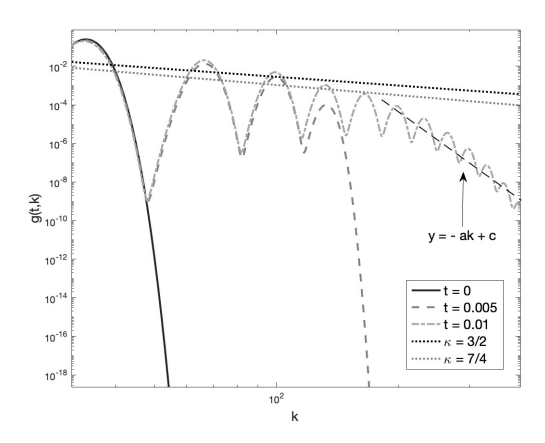


Fig. 4.11. Transient cascade corresponding to the initial condition (4.5).

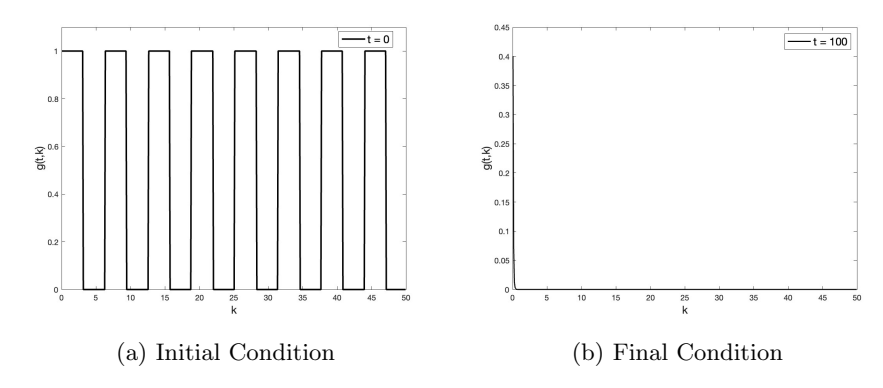


Fig. 4.12. Test case 3.

In Figure 4.12a we show the initial condition and in Figure 4.12b give the final state at T = 100. In the final state, it would appear that the remaining energy in the interval is collected near k = 0 with decreasing maximum amplitude at k = 0.05. It seems that this profile is maintained as  $T \to \infty$ , in a fashion similar to Tests 1 and 2.

We then vary the truncation parameter and show the decay of the energy for R=25,50,80 in Figure 4.13a. As mentioned previously, we can now see that the amount of energy increases with the interval size, but, importantly, the rate of decay is the same for each truncation value.

As in the previous tests, we explore varying the degree as seen in Figure 4.13b. Here, as in the next case, we begin to see further contrasting behavior compared with the previous two test cases. We see that the smaller the value of the degree, the longer the energy is conserved, but now, once the first blow-up time  $t_1^*$  is reached, the rate of decay is larger for  $\gamma = 3/2, 9/5$  compared to  $\gamma = 2$ . To see this, we add a reference line corresponding to a rate of decay like  $\mathcal{O}(\frac{1}{t})$  in Figures 4.13a and 4.13b. It would appear that for smaller values of  $\gamma$ , the decay rate is better described by  $\mathcal{O}(\frac{1}{t})$ , but for  $\gamma = 2$ , the theoretical bound  $\mathcal{O}(\frac{1}{\sqrt{t}})$  (see (1.8)) provides an excellent description of the cascade rate.

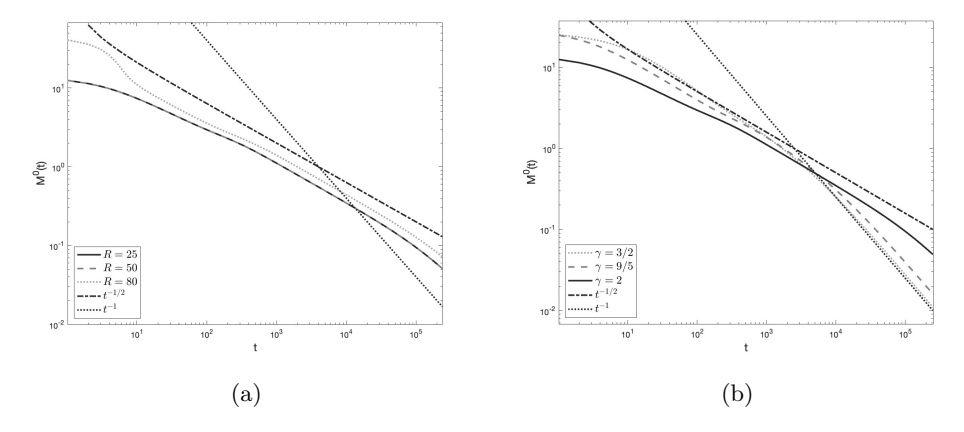


Fig. 4.13. (a) Zeroth moments of solution corresponding to initial condition (4.6), with  $\gamma=2$  and allowing R to vary. (b) Decay rate for initial condition (4.6) plotted against the theoretical rate. The red and black lines are translated to match the intersection of the moments.

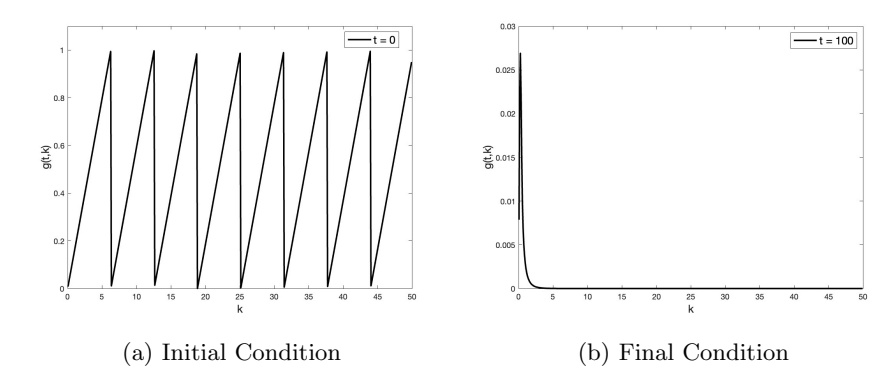


Fig. 4.14. Test case 4.

## **4.4.** Test **4.** Our last test has initial data given by

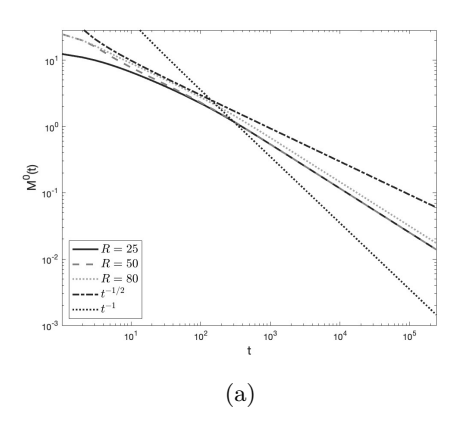
(4.7) 
$$g_0(k) = \frac{k - 2n\pi}{2\pi} \quad k \in [2n\pi, 2(n+1)\pi),$$

for  $n \in \mathbb{N}_0$ . As in Test 3, we set h = 0.1, T = 100, and  $\Delta t = 0.0004$  when R = 25 and R = 50 but  $\Delta t = 0.00025$  for R = 80.

We again give initial and final conditions in Figures 4.14a and 4.14b, respectively. As in Test 3, we observe that the energy is accumulated to a frequency nearer to k = 0 in some finite time  $T_s$ , where it remains fixed with decaying  $L^{\infty}$  norm.

Now fixing  $\gamma=2$  once again, we see in Figure 4.15a that varying the truncation parameter has a similar result on the total energy as in the previous test case. By extending the interval, we see that a larger amount of energy is retained but that the rate of decay is equal for all truncation values. Further, we see a good fit with the theoretical decay rate.

Next, we let  $\gamma = \frac{3}{2}, \frac{9}{5}, 2$  and keep R = 50 once again, and we show the zeroth moments of these solutions in Figure 4.15b. Here, as for the previous test cases, for  $\gamma = 3/2, 9/5$ , we see that the energy is conserved for a longer amount of time when



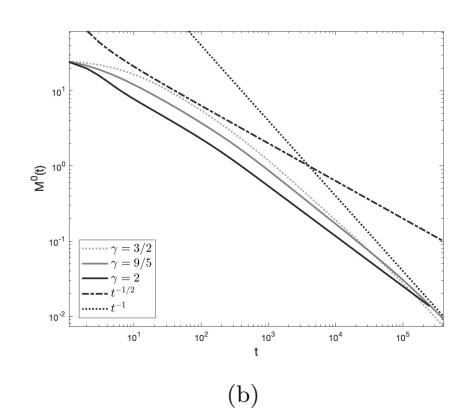


FIG. 4.15. (a) Zeroth moments of solution corresponding to initial condition (4.7), with  $\gamma=2$  and allowing R to vary. The theoretical decay rate is shown for comparison. (b) Zeroth moments of solution corresponding to initial condition (4.7), with R=50 and allowing  $\gamma$  to vary. The theoretical decay rate is shown for comparison.

compared to  $\gamma=2$ . As for the previous initial condition, it would appear that once the decay begins, the rates of decay are faster for  $\gamma=3/2,9/5$  than for  $\gamma=2$ . We again observe that for  $\gamma=2$ , the decay rate is more like  $\mathcal{O}(\frac{1}{\sqrt{t}})$ , and for the smaller values of  $\gamma$ , the decay rate is more like  $\mathcal{O}(\frac{1}{t})$ .

5. Conclusions and further discussion. We introduce a finite volume scheme which allows us to observe the long time asymptotics of the solutions of isotropic 3-wave kinetic equations, including the energy cascade behavior proved in [39]. Our numerical algorithm is based on the combination of the identity represented in Lemma 2.1 and Filbet and Laurençot's scheme [13] for the Smoluchowski coagulation equation.

From the four numerical tests, we can see that the energy cascade behavior happens for  $\gamma = \frac{3}{2}, \frac{9}{5}, 2$  and seems to verify the theory found in [39].

From the solutions computed in sections 4.1, 4.2, 4.3, and 4.4, one can see that the smaller  $\gamma$ , the slower the onset of decay. The energy cascade behavior also seems to occur independently of the smoothness of the initial data for all four cases with  $\gamma = \frac{3}{2}, \frac{9}{5}, 2$ .

The results in Figures 4.3 and 4.9 serve as another verification of the theory since the decay rate of the energy in any finite interval is the same due to the following fact proved in the main theorem of [39]:

$$\int_0^R g(t,\omega)d\omega = \int_{\mathbb{R}_+} \chi_{[0,R]}(\omega)g(t,\omega)d\omega \leq \ \mathcal{O}\Big(\frac{1}{\sqrt{t}}\Big) \text{ as } t \to \infty$$

for all truncation parameters R.

Therefore, the rate at which the energy leaves any finite interval [0, R] is the same since the convergence does not depend on the truncation parameter. As the theory is only for the energy cascade at the point  $\omega = \infty$ , it is a challenging task theoretically to obtain a convergence study pointwise with respect to all of the velocity variables in this  $\omega$ .

We would like to comment that in contrast to Tests 3 and 4, the amount of energy contained in the interval appears indistinguishable for the various truncation parameters in Tests 1 and 2. This can be explained by comparing  $||g^0||_{L^1(0,R)}$  of

the different test cases. The initial energy serves as a kind of reservoir in the finite intervals [30]. Then, for tests like Tests 3 and 4, we increase the amount of initial energy by increasing the size of the interval. That is, for  $R_1 < R_2 < R_3$  we have

This is not the case (or is negligible) for Tests 1 and 2, seen in Figures 4.3 and 4.9, due to the initial conditions selected there. The important thing to notice is that the slopes (decay rates) are independent of how much energy is contained in the interval initially, though the amount of energy can vary depending on the initial condition.

The numerical results confirm the theoretical bound (1.8) and show that the decay rate should be  $\mathcal{O}(\frac{1}{t^s})$ , with  $s \in [\frac{1}{2}, 1]$  for various initial data. In section 4.3, the cascade rate is described quite well by  $\mathcal{O}(\frac{1}{\sqrt{t}})$  for  $\gamma = 2$ . We then conclude that the cascade rate bound obtained in [39] is optimal.

**Acknowledgments.** The authors would like to thank Prof. T. Hagstrom for the use of SMU's high-performance computing cluster ManeFrame II (M2), Prof. B. Rumpf for his many crucial suggestions, and Prof. S. Nazarenko for several constructive suggestions which improved the numerical plots. The Los Alamos unlimited release number is LA-UR-23-20290.

## REFERENCES

- T. A. Bak and O. Heilmann, A finite version of Smoluchowski's coagulation equation, J. Phys. A, 24 (1991), pp. 4889–4893.
- [2] N. K. Bell, V. N. Grebenev, S. B. Medvedev, and S. V. Nazarenko, Self-similar evolution of Alfven wave turbulence, J. Phys. A, 50 (2017), 435501.
- [3] D. J. Benney and A. C. Newell, Random wave closures, Stud. Appl. Math., 48 (1969), pp. 29–53.
- [4] D. J. Benney and P. G. Saffman, Nonlinear interactions of random waves in a dispersive medium, Proc. R. Soc. Lond. A, 289 (1966), pp. 301–320.
- [5] T. Buckmaster, P. Germain, Z. Hani, and J. Shatah, Effective dynamics of the nonlinear Schrödinger equation on large domains, Comm. Pure Appl. Math., 71 (2018), pp. 1407– 1460.
- [6] C. COLLOT AND P. GERMAIN, Derivation of the Homogeneous Kinetic Wave Equation: Longer Time Scales, preprint, arXiv:2007.03508, 2020.
- [7] C. CONNAUGHTON, Numerical solutions of the isotropic 3-wave kinetic equation, Phys. D, 238 (2009), pp. 2282–2297.
- [8] C. CONNAUGHTON AND P. KRAPIVSKY, Aggregation-fragmentation processes and decaying threewave turbulence, Phys. Rev. E, 81 (2010), 035303.
- [9] C. Connaughton and A. C. Newell, Dynamical scaling and the finite-capacity anomaly in three-wave turbulence, Phys. Rev. E, 81 (2010), 036303.
- [10] F. P. DA COSTA, A finite-dimensional dynamical model for gelation in coagulation processes, J. Nonlinear Sci., 8 (1998), pp. 619-653.
- [11] Y. Deng and Z. Hani, Full Derivation of the Wave Kinetic Equation, preprint, arXiv:2104.11204, 2021.
- [12] A. DYMOV AND S. KUKSIN, Formal Expansions in Stochastic Model for Wave Turbulence 1: Kinetic Limit, preprint, arXiv:1907.04531, 2019.
- [13] F. FILBET AND P. LAURENÇOT, Numerical simulation of the Smoluchowski coagulation equation, SIAM J. Sci. Comput., 25 (2004), pp. 2004–2028, https://doi.org/10.1137/S1064827503429132.
- [14] E. L. FOSTER, J. LOHÉAC, AND M.-B. TRAN, A structure preserving scheme for the Kolmogorov-Fokker-Planck equation, J. Comput. Phys., 330 (2017), pp. 319–339, https://doi.org/10.1016/j.jcp.2016.11.009.
- [15] S. GALTIER, S. V. NAZARENKO, A. C. NEWELL, AND A. POUQUET, A weak turbulence theory for incompressible magnetohydrodynamics, J. Plasma Phys., 63 (2000), pp. 447–488.
- [16] I. M. GAMBA, L. M. SMITH, AND M.-B. TRAN, On the wave turbulence theory for stratified flows in the ocean, Math. Models Methods Appl. Sci., 30 (2020), pp. 105-137.

- [17] K. HASSELMANN, On the non-linear energy transfer in a gravity-wave spectrum I. General theory, J. Fluid Mech., 12 (1962), pp. 481–500.
- [18] K. HASSELMANN, On the spectral dissipation of ocean waves due to white capping, Bound.-Lay. Meteorol., 6 (1974), pp. 107–127.
- [19] X. Y. Hu, N. A. Adams, and C.-W. Shu, Positivity-preserving method for high-order conservative schemes solving compressible euler equations, J. Comput. Phys., 242 (2013), pp. 169–180.
- [20] J. Huang and C.-W. Shu, Positivity-preserving time discretizations for production-destruction equations with applications to non-equilibrium flows, J. Sci. Comput., 78 (2019), pp. 1811–1839.
- [21] J. Huang, W. Zhao, and C.-W. Shu, A third-order unconditionally positivity-preserving scheme for production-destruction equations with applications to non-equilibrium flows, J. Sci. Comput., 79 (2019), pp. 1015–1056.
- [22] B. B. Kadomtsev, Plasma Turbulence, Academic Press, New York, 1965.
- [23] D. D. KECK AND D. M. BORTZ, Numerical Simulation of Solutions and Moments of the Smoluchowski Coagulation Equation, preprint, arXiv:1312.7240, 2013.
- [24] A. O. KOROTKEVICH, A. I. DYACHENKO, AND V. E. ZAKHAROV, Numerical simulation of surface waves instability on a homogeneous grid, Phys. D, 321/322 (2016), pp. 51–66, https://doi.org/10.1016/j.physd.2016.02.017.
- [25] G. LAIBE AND M. LOMBART, On the Courant-Friedrichs-Lewy Condition for Numerical Solvers of the Coagulation Equation, preprint, arXiv:2109.11065, 2021.
- [26] R. J. LEVEQUE, Finite Difference Methods for Ordinary and Partial Differential Equations, SIAM, Philadelphia, 2007, https://doi.org/10.1137/1.9780898717839.
- [27] J. LUKKARINEN AND H. SPOHN, Weakly nonlinear Schrödinger equation with random initial data, Invent. Math., 183 (2011), pp. 79–188, https://doi.org/10.1007/s00222-010-0276-5.
- [28] Y. V. LVOV, K. L. POLZIN, E. G. TABAK, AND N. YOKOYAMA, Oceanic internal-wave field: Theory of scale-invariant spectra, J. Phys. Oceanogr., 40 (2010), pp. 2605–2623.
- [29] R. MICHA AND I. I. TKACHEV, Turbulent thermalization, Phys. Rev. D, 70 (2004), 043538.
- [30] S. NAZARENKO, Wave Turbulence, Lecture Notes in Physics 825, Springer, Heidelberg, 2011, https://doi.org/10.1007/978-3-642-15942-8.
- [31] T. T. NGUYEN AND M.-B. TRAN, On the kinetic equation in Zakharov's wave turbulence theory for capillary waves, SIAM J. Math. Anal., 50 (2018), pp. 2020–2047, https://doi.org/10.1137/17M1125042.
- [32] R. PEIERLS, Zur kinetischen Theorie der Wärmeleitung in Kristallen, Annalen der Physik, 395 (1929), pp. 1055-1101.
- [33] R. E. PEIERLS, Quantum theory of solids, in Theoretical Physics in the Twentieth Century: A Memorial Volume to Wolfgang Pauli, Interscience, New York, 1960, pp. 140–160.
- [34] Y. Pomeau and M.-B. Tran, Statistical Physics of Non Equilibrium Quantum Phenomena, Lecture Notes in Physics 967, Springer, Cham, 2019.
- [35] A. N. Pushkarev and V. E. Zakharov, Turbulence of capillary waves, Phys. Rev. Lett., 76 (1996), pp. 3320–3323.
- [36] A. N. Pushkarev and V. E. Zakharov, Turbulence of capillary waves: Theory and numerical simulation, Phys. D, 135 (2000), pp. 98-116.
- [37] B. RUMPF, A. SOFFER, AND M.-B. TRAN, On the Wave Turbulence Theory: Ergodicity for the Elastic Beam Wave Equation, 2021, submitted.
- [38] B. V. Semisalov, V. N. Grebenev, S. B. Medvedev, and S. V. Nazarenko, Numerical analysis of a self-similar turbulent flow in Bose-Einstein condensates, Commun. Nonlinear Sci., 102 (2021), 105903.
- [39] A. SOFFER AND M.-B. TRAN, On the energy cascade of 3-wave kinetic equations: Beyond Kolmogorov-Zakharov solutions, Commun. Math. Phys., (2019), pp. 1–48.
- [40] G. STAFFILANI AND M.-B. TRAN, On the Wave Turbulence Theory for a Stochastic KdV Type Equation, preprint, arXiv:2106.09819, 2021.
- [41] M.-B. Tran, G. Craciun, L. M. Smith, and S. Boldyrev, A reaction network approach to the theory of acoustic wave turbulence, J. Differential Equations, 269 (2020), pp. 4332–4352.
- [42] V. E. ZAKHAROV, Weak turbulence in media with a decay spectrum, J. Appl. Mech. Tech. Phys., 6 (1965), pp. 22–24.
- [43] V. E. Zakharov, Stability of periodic waves of finite amplitude on the surface of a deep fluid, J. Appl. Mech. Tech. Phys., 9 (1968), pp. 190-194.

- [44] V. E. Zakharov and N. N. Filonenko, Weak turbulence of capillary waves, J. Appl. Mech. Tech. Phys., 8 (1967), pp. 37–40.
- [45] V. E. ZAKHAROV, V. S. L'VOV, AND G. FALKOVICH, Kolmogorov Spectra of Turbulence I: Wave Turbulence, Springer, Berlin, 2012.
- [46] V. E. ZAKHAROV AND S. V. NAZARENKO, Dynamics of the Bose-Einstein condensation, Phys. D, 201 (2005), pp. 203–211, https://doi.org/10.1016/j.physd.2004.11.017.